The exact equivalence of the one-flavour lattice Thirring model with Wilson fermions to a two-colour loop model

K. Scharnhorst[†]

University of Wales Swansea
Department of Physics
Singleton Park
Swansea, SA2 8PP
United Kingdom

and

Humboldt-Universität zu Berlin[‡]
Institut für Physik
Invalidenstr. 110
D-10115 Berlin
Federal Republic of Germany

Abstract

Within Euclidean lattice field theory an exact equivalence between the one-flavour 2D Thirring model with Wilson fermions and Wilson parameter $r = 1$ to a two-colour loop model on the square lattice is established. For non-interacting fermions this model reduces to an exactly solved loop model which is known to be a free fermion model. The two-colour loop model equivalent to the Thirring model can also be understood as a 4-state 49-vertex model.

[†]E-mail: `scharnh@linde.physik.hu-berlin.de`
[‡]Present address

1 Introduction

Four-fermion models on the lattice and in the continuum (in various dimensions) have received a great deal of attention in recent years. This interest is related to the problem of dynamical symmetry breaking [1], [2] as well as to the possible role of four-fermion interactions in QED in 4D [3], [4]. However, the reliable investigation of these models requires the application of non-perturbative and exact methods which are hard to come by. Within lattice field theory the investigation of fermionic theories is hampered by the notorious difficulties encountered in their numerical simulation, in particular, when the number of fermion species involved is odd. The development of new methods for this class of theories is therefore highly desirable.

Following a method developed by Salmhofer [5] in the exact study of the one-flavour strong-coupling lattice Schwinger model with Wilson fermions, we have recently suggested [6] that this method can also be applied to a wide class of purely fermionic theories with Wilson fermions in various dimensions. The study of the one- and two-flavour strong-coupling Schwinger models has lead to exact equivalences to statistical models which can be understood as either q-state vertex models or loop models [5], [6]. In contrast to strongly coupled gauge theories with staggered fermions, which lead to pure monomer-dimer systems [7], the consideration of Wilson fermions results in a different class of model, as these examples demonstrate.

In the present article, as a first step towards the application of the new method to four-fermion theories, within Euclidean lattice field theory we investigate the one-flavour 2D Thirring model with Wilson fermions. In the past decades the one-flavour Thirring model in 2D has been widely studied in the continuum as well as within the Hamiltonian lattice approach. The massive Thirring model in the continuum is known to be quantum integrable ([8], see also [9]) and to be equivalent to the sine-Gordon model [10]. Within the Hamiltonian lattice approach equivalences of the Thirring model to other statistical models have been found previously [11], [12] (see also the references cited in [9]). These models are related to staggered fermions. The only attempt so far to study the one-flavour Thirring model with multi-component spinors has been made by Ishida and Saito [13]. They however consider the case of naive fermions ('Wilson fermions with Wilson parameter $r = 0$') only, which turns out to be much more involved than the case of Wilson fermions with $r = 1$ we are going to investigate in the present article.

The method we will employ is based on the fact that the Grassmann integration on the lattice can be performed exactly. The Grassmann integration will consecutively be carried out on the even and odd sublattices. In this process the possible contributions to the partition function will be analyzed (for the method see also [5],

[6]). In order to simplify the required algebraic manipulations with Grassmann variables we make use of a Mathematica program [14] specially designed for the present purpose. Since we consider only one fermion species, throughout the paper we pay careful attention to the ordering problem for the Grassmann variables involved in order to keep track of any minus signs which possibly might lead to negative contributions to the partition function.

The plan of the article is as follows. The main investigation is presented in section 2 which is divided into several subsections. This division is introduced in order to give the reader easier access to the different steps in establishing the transformation from the one-flavour lattice Thirring model with Wilson fermions to the equivalent statistical model. The structure of section 2 is explained in further detail at the end of its introductory part (before subsection 2.1 starts). Section 3 contains some discussion and conclusions. Finally, the proof of a mathematical result needed in subsection 2.2 is deferred to an Appendix.

2 The loop model equivalence

The partition function Z_Λ of the one-flavour Thirring model with Wilson fermions on the square lattice Λ is given by

$$Z_\Lambda = \int D\psi D\bar{\psi} \; \mathrm{e}^{-S} \quad , \tag{1}$$

where $D\psi D\bar{\psi} = \prod_{x \in \Lambda} d\psi_1(x) \, d\bar{\psi}_1(x) \, d\psi_2(x) \, d\bar{\psi}_2(x)$ denotes the multiple Grassmann integration on the lattice (The subscripts are spinor indices.). The action S is defined by

$$S = \sum_{x \in \Lambda} \left(\frac{1}{2} \sum_\mu \left(\bar{\psi}(x + e_\mu)(1 + \gamma_\mu)\psi(x) + \bar{\psi}(x)(1 - \gamma_\mu)\psi(x + e_\mu) \right) \right.$$

$$\left. - M\bar{\psi}(x)\psi(x) - \frac{G}{2} \, J_\mu(x)J_\mu(x) \right) \tag{2}$$

with

$$J_\mu(x) = \bar{\psi}(x)\gamma_\mu\psi(x) \quad , \tag{3}$$

$$J_\mu(x)J_\mu(x) = 4 \, \bar{\psi}_1(x)\bar{\psi}_2(x)\psi_1(x)\psi_2(x) \quad . \tag{4}$$

In eq. (2) the Wilson parameter r has been set to 1; the hopping parameter κ is consequently given by $\kappa = 1/2M$. Eq. (1) can be written as follows.

$$
\begin{aligned}
Z_\Lambda \;=\; & \sum_{k_l \in \{0,1,2,3,4\}} \int D\psi D\bar{\psi} \ \exp\left(\sum_{x \in \Lambda} M\bar{\psi}(x)\psi(x) \right) \\[2mm]
& \times \ \exp\left(2G \sum_{x \in \Lambda} \bar{\psi}_1(x)\bar{\psi}_2(x)\psi_1(x)\psi_2(x) \right) \\[2mm]
& \times \prod_{l=(x,x+e_\mu)} \frac{1}{k_l!} \left[\bar{\psi}(x+e_\mu)T_\mu^{(+)}\psi(x) + \bar{\psi}(x)T_\mu^{(-)}\psi(x+e_\mu) \right]^{k_l}. \quad (5)
\end{aligned}
$$

The occupation numbers k_l cannot exceed 4 because on each lattice site only 4 Grassmann variables are present. Explicit calculation however shows that by virtue of the nilpotency of the Grassmann variables k_l cannot exceed 2 (This is closely related to the fact that we have employed $r = 1$.). As in [5], we choose $\gamma_1 = \sigma_3$, $\gamma_2 = \sigma_1$ (σ_i are Pauli matrices.) and the projection operators $T_\mu^{(\epsilon)} = (1 + \epsilon\gamma_\mu)/2$, $\epsilon \in \{-1, 1\}$ then read $T_1^{(+)} = \mathrm{diag}\{1, 0\}$, $T_1^{(-)} = \mathrm{diag}\{0, 1\}$, $T_2^{(\epsilon)} = \frac{1}{2}\begin{pmatrix} 1 & \epsilon \\ \epsilon & 1 \end{pmatrix}$. It is now advantageous in order to simplify further results to define combinations of the original ψ fields in terms of which $T_2^{(\epsilon)}$ is diagonal

$$
\chi(x) \;=\; U\psi(x) \;=\; \frac{1}{\sqrt{2}} \left(\psi_1(x) + \psi_2(x), \psi_1(x) - \psi_2(x) \right)^T \quad , \tag{6}
$$

$$
\bar{\chi}(x) \;=\; \bar{\psi}(x)U \;=\; \frac{1}{\sqrt{2}} \left(\bar{\psi}_1(x) + \bar{\psi}_2(x), \bar{\psi}_1(x) - \bar{\psi}_2(x) \right) \tag{7}
$$

with

$$
U \;=\; \frac{1}{\sqrt{2}} \begin{pmatrix} 1 & 1 \\ 1 & -1 \end{pmatrix} \;=\; U^{-1} \quad . \tag{8}
$$

The discussion in this section proceeds via the following steps indicated by subsections. In subsection 2.1, the Grassmann integration is carried out exactly in two steps, first on the even and then on the odd sublattices. In this process, a procedure based on graphical elements (vertices) is established for describing the results. Combinations of these graphical elements (vertex clusters) stand in correspondence to contributions to the partition function (sum) Z_Λ. In subsection 2.2, rules for the calculation of the weight of the contribution of an arbitrary vertex cluster are discussed. In subsection 2.3, the fact that the weight of certain vertex clusters may vanish (due

to certain cancellations among different terms contributing to the partition function) is exploited to interpret the graphical rules established in subsection 2.1 in terms of a loop model picture. This finally allows to specify in subsection 2.4 the statistical model equivalent to the one-flavour lattice Thirring model with Wilson fermions.

2.1   The result of the Grassmann integration

In the expression for the partition function (5) the integration on the even sublattice Λ_e is now performed first. As each lattice site x supports 4 Grassmann variables terms which respect

$$\sum_{l \ni x} k_l \ + \ 2s_x \ + 4t_x \ = \ 4 \tag{9}$$

can give a non-vanishing contribution only ($s_x = 0, 1, 2$ is the power of $M\bar{\psi}(x)\psi(x)$ and $t_x = 0, 1$ is the power of $2G\bar{\psi}_1(x)\bar{\psi}_2(x)\psi_1(x)\psi_2(x)$ in the expansion of the exponentials in eq. (5).). Below we give the results for all local integrals related to a given lattice site $x \in \Lambda_e$ which allow non-vanishing contributions. We have relied on a purpose-written Mathematica program [14] to do the necessary algebra. The results have been arranged in a way most suitable for the further discussion. The graphical rules below have to be interpreted as follows: the black dot denotes any point x on the even sublattice Λ_e at which the Grassmann integration is performed, a dashed line means $k_l = 0$ while thin and thick lines stand for $k_l = 1$ and $k_l = 2$ respectively. A vertex is understood to be a lattice point with certain admissible values of the occupation numbers k_l on the attached links. A given set of occupation numbers k_l on the lattice Λ uniquely determines a certain diagram denoting a contribution to the partition function (As one can see from eq. (10), we consider the cases $s_x = 2, t_x = 0$ and $s_x = 0, t_x = 1$ as unified into one.). Finally, the first coordinate component of x is understood to be the horizontal one while the second component runs vertically.

There is one possible vertex with $s_x = 2$ or $t_x = 1$:

Vertex 1

$$\text{---}\!\!\!+\!\!\!\text{---} \ \ = \ \ \int \prod_{\alpha=1}^{2} d\psi_\alpha(x) \, d\bar{\psi}_\alpha(x) \, \left\{ \frac{1}{2} \left(M\bar{\psi}(x)\psi(x) \right)^2 \right.$$

$$\left. + \ 2 \, G \ \bar{\psi}_1(x)\bar{\psi}_2(x)\psi_1(x)\psi_2(x) \right\}$$

$$= \ \ M^2 - 2 \, G \tag{10}$$

5

All further vertices have $s_x = 0$ (vertices 2-20) or $s_x = 1$ (vertices 21-26) and $t_x = 0$
(The results for the vertices 2-7 can also be found in the paper by Salmhofer [5],
including the explicit steps of the derivation of the r.h.s. of eqs. (12) and (14).).

Vertex 2

$$\chi_1(x - e_2) \; \bar{\chi}_1(x + e_2) \; \chi_2(x + e_2) \; \bar{\chi}_2(x - e_2) \tag{11}$$

Vertex 3

$$\psi_1(x - e_1) \; \bar{\psi}_1(x + e_1) \; \psi_2(x + e_1) \; \bar{\psi}_2(x - e_1) \tag{12}$$

Vertex 4

$$- \; \psi_2(x + e_1) \; \bar{\chi}_2(x - e_2) \; \chi_1(x - e_2) \; \bar{\psi}_1(x + e_1)/2 \tag{13}$$

Vertex 5

$$- \; \psi_1(x - e_1) \; \bar{\chi}_1(x + e_2) \; \chi_2(x + e_2) \; \bar{\psi}_2(x - e_1)/2 \tag{14}$$

Vertex 6

$$\psi_2(x + e_1) \; \bar{\chi}_1(x + e_2) \; \chi_2(x + e_2) \; \bar{\psi}_1(x + e_1)/2 \tag{15}$$

Vertex 7

$$\psi_1(x - e_1) \; \bar{\chi}_2(x - e_2) \; \chi_1(x - e_2) \; \bar{\psi}_2(x - e_1)/2 \tag{16}$$

Vertex 8

$$= \quad [\psi_1(x - e_1) \, \bar{\chi}_1(x + e_2) \, \chi_1(x - e_2) \, \bar{\psi}_2(x - e_1)$$
$$- \, \psi_1(x - e_1) \, \bar{\chi}_2(x - e_2) \, \chi_2(x + e_2) \, \bar{\psi}_2(x - e_1)]/2 \qquad (17)$$

Vertex 9

$$= \quad [\psi_2(x + e_1) \, \bar{\chi}_1(x + e_2) \, \chi_1(x - e_2) \, \bar{\psi}_1(x + e_1)$$
$$- \, \psi_2(x + e_1) \, \bar{\chi}_2(x - e_2) \, \chi_2(x + e_2) \, \bar{\psi}_1(x + e_1)]/2 \qquad (18)$$

Vertex 10

$$= \quad [\chi_2(x + e_2) \, \bar{\psi}_1(x + e_1) \, \psi_1(x - e_1) \, \bar{\chi}_1(x + e_2)$$
$$- \, \chi_2(x + e_2) \, \bar{\psi}_2(x - e_1) \, \psi_2(x + e_1) \, \bar{\chi}_1(x + e_2)]/2 \qquad (19)$$

Vertex 11

$$= \quad [\chi_1(x - e_2) \, \bar{\psi}_1(x + e_1) \, \psi_1(x - e_1) \, \bar{\chi}_2(x - e_2)$$
$$- \, \chi_1(x - e_2) \, \bar{\psi}_2(x - e_1) \, \psi_2(x + e_1) \, \bar{\chi}_2(x - e_2)]/2 \qquad (20)$$

Vertex 12

$$= \quad [\psi_1(x - e_1) \, \bar{\psi}_1(x + e_1) \, \chi_1(x - e_2) \, \bar{\psi}_2(x - e_1)$$
$$+ \, \psi_1(x - e_1) \, \bar{\chi}_2(x - e_2) \, \psi_2(x + e_1) \, \bar{\psi}_2(x - e_1)]/\sqrt{2} \qquad (21)$$

Vertex 13

$$
\begin{aligned}
= \quad & [\chi_2(x+e_2)\,\bar{\psi}_1(x+e_1)\,\chi_1(x-e_2)\,\bar{\chi}_1(x+e_2) \\
& + \chi_2(x+e_2)\,\bar{\chi}_2(x-e_2)\,\psi_2(x+e_1)\,\bar{\chi}_1(x+e_2)]/\sqrt{2}
\end{aligned}
\tag{22}
$$

Vertex 14

$$
\begin{aligned}
= \quad & [\psi_2(x+e_1)\,\bar{\psi}_2(x-e_1)\,\chi_2(x+e_2)\,\bar{\psi}_1(x+e_1) \\
& + \psi_2(x+e_1)\,\bar{\chi}_1(x+e_2)\,\psi_1(x-e_1)\,\bar{\psi}_1(x+e_1)]/\sqrt{2}
\end{aligned}
\tag{23}
$$

Vertex 15

$$
\begin{aligned}
= \quad & [\chi_1(x-e_2)\,\bar{\psi}_2(x-e_1)\,\chi_2(x+e_2)\,\bar{\chi}_2(x-e_2) \\
& + \chi_1(x-e_2)\,\bar{\chi}_1(x+e_2)\,\psi_1(x-e_1)\,\bar{\chi}_2(x-e_2)]/\sqrt{2}
\end{aligned}
\tag{24}
$$

Vertex 16

$$
\begin{aligned}
= \quad & [-\,\psi_1(x-e_1)\,\bar{\psi}_1(x+e_1)\,\chi_2(x+e_2)\,\bar{\psi}_2(x-e_1) \\
& + \psi_1(x-e_1)\,\bar{\chi}_1(x+e_2)\,\psi_2(x+e_1)\,\bar{\psi}_2(x-e_1)]/\sqrt{2}
\end{aligned}
\tag{25}
$$

Vertex 17

$$
\begin{aligned}
= \quad & [\chi_1(x-e_2)\,\bar{\psi}_1(x+e_1)\,\chi_2(x+e_2)\,\bar{\chi}_2(x-e_2) \\
& - \chi_1(x-e_2)\,\bar{\chi}_1(x+e_2)\,\psi_2(x+e_1)\,\bar{\chi}_2(x-e_2)]/\sqrt{2}
\end{aligned}
\tag{26}
$$

Vertex 18

$$\begin{aligned}
\text{(diagram)} \quad = \quad & [- \chi_2(x + e_2)\ \bar{\psi}_2(x - e_1)\ \chi_1(x - e_2)\ \bar{\chi}_1(x + e_2) \\
& + \chi_2(x + e_2)\ \bar{\chi}_2(x - e_2)\ \psi_1(x - e_1)\ \bar{\chi}_1(x + e_2)]/\sqrt{2}
\end{aligned} \tag{27}$$

Vertex 19

$$\begin{aligned}
\text{(diagram)} \quad = \quad & [\psi_2(x + e_1)\ \bar{\psi}_2(x - e_1)\ \chi_1(x - e_2)\ \bar{\psi}_1(x + e_1) \\
& - \psi_2(x + e_1)\ \bar{\chi}_2(x - e_2)\ \psi_1(x - e_1)\ \bar{\psi}_1(x + e_1)]/\sqrt{2}
\end{aligned} \tag{28}$$

Vertex 20

$$\begin{aligned}
\text{(diagram)} \quad = \quad - [\quad & \chi_1(x - e_2)\ \bar{\psi}_1(x + e_1)\ \chi_2(x + e_2)\ \bar{\psi}_2(x - e_1) \\
& + \psi_1(x - e_1)\ \bar{\chi}_1(x + e_2)\ \chi_1(x - e_2)\ \bar{\psi}_1(x + e_1)/2 \\
& + \psi_1(x - e_1)\ \bar{\chi}_2(x - e_2)\ \chi_2(x + e_2)\ \bar{\psi}_1(x + e_1)/2 \\
& + \psi_2(x + e_1)\ \bar{\chi}_1(x + e_2)\ \chi_1(x + e_2)\ \bar{\psi}_2(x - e_1)/2 \\
& + \psi_2(x + e_1)\ \bar{\chi}_2(x - e_2)\ \chi_2(x + e_2)\ \bar{\psi}_2(x - e_1)/2 \\
& + \psi_1(x - e_1)\ \bar{\chi}_1(x + e_2)\ \psi_2(x + e_1)\ \bar{\chi}_2(x - e_2)]
\end{aligned} \tag{29}$$

Vertex 21

$$\text{(diagram)} \quad = \quad M\ [\chi_1(x - e_2)\ \bar{\chi}_1(x + e_2)\ +\ \chi_2(x + e_2)\ \bar{\chi}_2(x - e_2)] \tag{30}$$

Vertex 22

$$\text{(diagram)} \quad = \quad M\ [\psi_1(x - e_1)\ \bar{\psi}_1(x + e_1)\ +\ \psi_2(x + e_1)\ \bar{\psi}_2(x - e_1)] \tag{31}$$

Vertex 23

$$\text{---}\hspace{-0.5em}\bullet\hspace{-0.3em}\text{|---} \qquad = \quad M \, [\chi_1(x - e_2) \, \bar{\psi}_1(x + e_1) \; - \; \psi_2(x + e_1) \, \bar{\chi}_2(x - e_2)]/\sqrt{2} \qquad (32)$$

Vertex 24

$$\text{---}\hspace{-0.5em}\bullet\hspace{-0.3em}\text{---} \qquad = \quad M \, [\psi_1(x - e_1) \, \bar{\chi}_1(x + e_2) \; - \; \chi_2(x + e_2) \, \bar{\psi}_2(x - e_1)]/\sqrt{2} \qquad (33)$$

Vertex 25

$$\text{---}\hspace{-0.5em}\bullet\hspace{-0.3em}\text{|---} \qquad = \quad M \, [\chi_2(x + e_2) \, \bar{\psi}_1(x + e_1) \; + \; \psi_2(x + e_1) \, \bar{\chi}_1(x + e_2)]/\sqrt{2} \qquad (34)$$

Vertex 26

$$\text{---}\hspace{-0.5em}\bullet\hspace{-0.3em}\text{---} \qquad = \quad M \, [\chi_1(x - e_2) \, \bar{\psi}_2(x - e_1) \; + \; \psi_1(x - e_1) \, \bar{\chi}_2(x - e_2)]/\sqrt{2} \qquad (35)$$

In order to achieve further understanding it is useful to assign the remaining $\bar{\psi}$, ψ fields on the odd sublattice Λ_o certain graphical symbols as follows (The full black dot denotes a point x on the even sublattice while the hollow circle stands for the point on the odd sublattice which the argument of the fields relates to.).

$$\circ\!\!-\!\!\!\rightarrow\!\!\bullet \quad = \quad \bar{\psi}_2(x - e_1) \qquad (36) \qquad \circ\!\!\rightarrow\!\!\!-\!\!\bullet \quad = \quad \psi_1(x - e_1) \qquad (37)$$

$$\bullet\!\!-\!\!\!\rightarrow\!\!\circ \quad = \quad \psi_2(x + e_1) \qquad (38) \qquad \bullet\!\!\leftarrow\!\!\!-\!\!\circ \quad = \quad \bar{\psi}_1(x + e_1) \qquad (39)$$

$$\begin{matrix}\bullet \\ | \\ \circ\end{matrix} \quad = \quad \bar{\chi}_2(x - e_2) \qquad (40) \qquad \begin{matrix}\bullet \\ | \\ \circ\end{matrix} \quad = \quad \chi_1(x - e_2) \qquad (41)$$

$$\begin{matrix}\circ \\ | \\ \bullet\end{matrix} \quad = \quad \chi_2(x + e_2) \qquad (42) \qquad \begin{matrix}\circ \\ | \\ \bullet\end{matrix} \quad = \quad \bar{\chi}_1(x + e_2) \qquad (43)$$

As a rule, an arrow flowing out of a point of the odd sublattice (hollow circles) de-

10

notes a $\bar{\psi}$, $\bar{\chi}$ field variable while an arrow flowing into a point on the odd sublattice relates to a ψ, χ field variable. From this it is already clear that only those products of (four) Grassmann fields at any point of the odd sublattice allow non-vanishing contributions to the partition function Z_Λ which have two incoming and two outgoing arrows in their graphical symbols. We will refer to this fact as the vertex arrow rule. The symbols for the fields on the odd sublattice can now be used in a natural way to construct further graphical building blocks. As will become clear further below we choose signs in accordance with eqs. (30)-(35) (for $M = 1$).

$$= \qquad \chi_2(x + e_2)\, \bar{\chi}_2(x - e_2) \quad + \quad \chi_1(x - e_2)\, \bar{\chi}_1(x + e_2) \qquad (44)$$

$$= \qquad \psi_2(x + e_1)\, \bar{\psi}_2(x - e_1) \quad + \quad \psi_1(x - e_1)\, \bar{\psi}_1(x + e_1) \qquad (45)$$

$$= \qquad \chi_1(x - e_2)\, \bar{\psi}_1(x + e_1)/\sqrt{2} \quad - \quad \psi_2(x + e_1)\, \bar{\chi}_2(x - e_2)/\sqrt{2} \qquad (46)$$

$$= \qquad \psi_1(x - e_1)\, \bar{\chi}_1(x + e_2)/\sqrt{2} \quad - \quad \chi_2(x + e_2)\, \bar{\psi}_2(x - e_1)/\sqrt{2} \qquad (47)$$

$$= \qquad \psi_2(x + e_1)\, \bar{\chi}_1(x + e_2)/\sqrt{2} \quad + \quad \chi_2(x + e_2)\, \bar{\psi}_1(x + e_1)/\sqrt{2} \qquad (48)$$

11

$$\text{[diagram]} \quad = \quad \frac{1}{\sqrt{2}} \quad \text{[diagram]} \quad + \frac{1}{\sqrt{2}} \quad \text{[diagram]}$$

$$= \quad \chi_1(x - e_2)\, \bar{\psi}_2(x - e_1)/\sqrt{2} \; + \; \psi_1(x - e_1)\, \bar{\chi}_2(x - e_2)/\sqrt{2} \qquad (49)$$

One immediately recognizes the significance of the numerical factors for each vertex. The rule simply is that each corner element (46)-(49) is associated with a factor $1/\sqrt{2}$. Using the above pictorial language for the remaining fields and their combinations on the odd sublattice we can gain now already some intuitive understanding for the structures appearing on the r.h.s. of eqs. (11)-(29) by interpreting them in terms of the graphical symbols introduced in eqs. (36)-(43), (44)-(49). We give some characteristic examples; similar relations can also be obtained for the omitted vertices.

Vertex 3

$$\text{[diagram]} \quad = \quad \frac{1}{2} \quad \text{[diagram]} \; \times \; \text{[diagram]} \quad = \quad \text{[diagram]} \; \times \; \text{[diagram]} \qquad (50)$$

Vertex 6

$$\text{[diagram]} \quad = \quad \frac{1}{2} \quad \text{[diagram]} \; \times \; \text{[diagram]} \quad = \quad \frac{1}{2} \quad \text{[diagram]} \; \times \; \text{[diagram]} \qquad (51)$$

Since the vertices 8-20 correspond to sums of field products the following condensed notation is appropriate. Each of the pictures below however can also be expanded in terms of oriented line segments.

Vertex 10

$$\text{[diagram]} \quad = \quad \text{[diagram]} \; \times \; \text{[diagram]} \qquad (52)$$

Vertex 14

$$\text{[diagram]} \quad = \quad \text{[diagram]} \; \times \; \text{[diagram]} \qquad (53)$$

Vertex 20

$$\tag{54}$$

It should be mentioned that most of the above relations (50)-(54) do not generalize to the case when the Wilson parameter r is chosen not to be 1. However, interestingly enough eq. (54) still applies for $r \neq 1$ if for the graphical symbols (44)-(49) the expressions then obtained for the vertices 21-26 (eqs. (30)-(35)) are inserted (with $M = 1$).

What remains to be done now is to discuss the result for the Grassmann integration on the odd sublattice Λ_o. For the moment we exclude vertex 20 (and its equivalent on the odd sublattice) from consideration as its complexity requires special attention. It will be discussed at a later stage, in subsection 2.2. Now, it is useful to introduce a graphical notation for the product of two field variables at a certain point x of the odd sublattice Λ_o. In view of the vertex arrow rule we only need products of two Grassmann fields where one of them carries a bar (i.e. oriented line segments in the pictorial language). We order the products always in such a way that for a given lattice point the out-arrow field variable stands first (For points on the odd sublattice this entails that the bar variable is the first factor in a product while for points on the even lattice it is always the second factor; see e.g. the ordering applied in eqs. (11)-(35).). We give just an example; all other combinations are defined in an analogous way (see eqs. (36)-(43) for the notation).

$$\bullet\!\!-\!\!\circ\!\!-\!\!\bullet \quad = \quad \bar{\psi}_1(x)\,\psi_1(x) \tag{55}$$

It is also useful to establish a graphical symbol for the mass term combination of the fields.

$$\bigcirc \quad = \quad M\left[\bar{\psi}_1(x)\,\psi_1(x)\ +\ \bar{\psi}_2(x)\,\psi_2(x)\right] \tag{56}$$

Using these symbols we can now conveniently discuss the Grassmann integration on the odd sublattice Λ_o. The graphical symbols below denote in an intuitive way the product of (four) Grassmann variables (and sums of them in eqs. (63)-(65)). The ordering is performed within pairs of fields which stand for an oriented line segment.

13

In each pair the bar variable stands first. As these products of two Grassmann variables are Grassmann even, no further ordering prescription is required. The black dot in the hollow circle of the point on the odd sublattice Λ_o (which is the central point in the diagrams below) indicates that the Grassmann integration has now been performed. In view of the vertex arrow rule one finds the following non-zero results (Dots which are close together denote one and the same lattice point). We give some characteristic examples only.

$$\text{(diagram)} \quad = \int \prod_{\alpha=1}^{2} d\psi_\alpha(x) \, d\bar{\psi}_\alpha(x) \, \bar{\psi}_1(x) \, \psi_1(x) \, \bar{\psi}_2(x) \, \psi_2(x) \quad = \quad 1 \tag{57}$$

$$\text{(diagram)} \quad = \quad -\frac{1}{2} \tag{58}$$

$$\text{(diagram)} \quad = \quad \frac{1}{2} \tag{59}$$

$$\text{(diagram)} \quad = \quad - \quad \text{(diagram)} \quad = \frac{1}{2} \tag{60}$$

$$\text{(diagram)} \quad = \quad \text{(diagram)} \quad = \frac{1}{\sqrt{2}} \tag{61}$$

$$\text{(diagram)} \quad = \quad - \quad \text{(diagram)} \quad = \frac{1}{\sqrt{2}} \tag{62}$$

$$\text{(diagram)} \quad = \quad \text{(diagram)} \quad = M \tag{63}$$

$$\text{(diagram)} \quad = \quad - \quad \text{(diagram)} \quad = \frac{M}{\sqrt{2}} \tag{64}$$

$$\text{(diagram)} \quad = \quad \text{(diagram)} \quad = \frac{M}{\sqrt{2}} \tag{65}$$

It is interesting to note that the results (61), (63), (65) are symmetric under arrow exchange, while those for (60), (62), (64) are antisymmetric. This consideration can also be extended to the vertices (17)-(28), (30)-(35) on the even sublattice Λ_e, when

the graphical symbols (36)-(43) are also used there. For the moment, we denote the different terms in (17)-(28), (30)-(35) as subvertices. One finds that the subvertices on the even sublattice have exactly the same symmetry properties with respect to arrow reversal as their counterparts on the odd sublattice.

2.2   The calculation of vertex cluster weights

In order to gain further insight into the structures under study it is useful to consider in eqs. (11)-(28), (30)-(35) the numerical factor in front of a given product of four Grassmann variables (where the sign is fixed by the ordering prescription used) as weight of a given subvertex (combination of oriented line segments) on the even sublattice Λ_e. One then observes that the subvertices (products) in (11)-(28), (30)-(35) have exactly the same weights as their counterparts on the odd sublattice Λ_o (cf. eqs. (57)-(65)). Consequently, from now on the distinction between even and odd sublattice vertices will no longer play any role (except in the discussion of vertex 20 given further below). Furthermore, one can convince oneself that their weights can easily be given by means of a simple rule. Each oriented line segment can be associated with a certain weight ($+1$ for straight lines, $\pm 1/\sqrt{2}$ for bent lines). The weight for any particular line segment can be read from the upper lines in eqs. (44)-(49). The weights in vertices 2-19 (eqs. (11)-(28)) can then be calculated by simply representing them by two oriented line segments (thick lines are understood as two thin lines with opposite orientations) and then multiplying the weights of these line segments. For example, this way one obtains from (46), (47) the negative sign on the r.h.s. of (13), (14). To obtain the weights in (30)-(35) one simply multiplies the line segment weights by another factor of M. The same rule applies to eqs. (57)-(65).

We are now almost prepared to calculate the weight of any given vertex cluster (i.e. a connected diagram built of the vertices 2-26). One remaining subject to be discussed is whether our above ordering prescriptions for products of odd sublattice Grassmann fields related to the vertices on the even and odd sublattices are compatible. As each cluster can be understood as consisting of a certain number of thin line loops we may study the ordering problem separately for a single loop (For this purpose we consider thick lines as two oppositely oriented thin lines.). With an eye to eq. (5), one may now easily convince oneself that if for the even sublattice vertices the ordering prescription applied in eqs. (11)-(28), (30)-(35) is used one need not to reorder the Grassmann variables related to the odd sublattice points in order to obey the ordering prescription used in eqs. (57)-(65) except for one arbitrarily selected point in any single loop. Consequently, each thin line loop contributes an additional factor of -1, characteristic of any fermion loop in field theory, arising from ordering effects. Consequently, thick line loops do not contribute any minus sign

because they can be understood as two thin line loops.

After the above discussion it is now straightforward to also analyze vertex clusters which contain the vertex 20 (and its analogue on the odd sublattice) we omitted so far. The remarkable eq. (54) immediately suggests how to proceed. Each vertex 20 can be split into three different diagrams where the vertex is interpreted within the loop picture according to the graphical symbols on the r.h.s. of eq. (54), and then one may proceed exactly as for vertex clusters without vertex 20 (In total we have $(3 \times 4 =)$ twelve, in part identical, products of Grassmann fields with different loop picture interpretations attached to them, i.e. four products for each of the three terms on the r.h.s. of eq. (54).). However, eq. (54) stands for a vertex 20 on the even sublattice Λ_e and it remains to be seen whether an analogous interpretation is possible for the analogue of vertex 20 on the odd sublattice Λ_o. The results for it read as follows (We here apply the same conventions as in eqs. (57)-(65).).

$$= -1 \qquad (66)$$

$$= -\frac{1}{2} \qquad (67)$$

In the above equations for ordering purposes we have applied a certain interpretation in terms of oriented line segments. However, each of the above six pictures allows two different interpretations in terms of oriented line segments (leading in total again to twelve different graphical terms). Consequently, one may decide to apply one ordering in a certain fraction $\alpha \in \mathbf{R}$ of cases (i.e. for those cases shown in (66), (67)) and in another fraction $(1-\alpha)$ the other, alternative prescription. The weight for each subvertex then has to be multiplied by α or $(1-\alpha)$ respectively in order to obtain the correct final result for the partition function. The two vertices in eq. (66) can both be interpreted in an alternative way (relative to the one shown in eq. (66)) as two oriented bent line segments passing each other without intersection. The four vertices in eqs. (67) each allow an interpretation as either two oriented bent line segments passing each other without intersection (as shown) or as two oriented straight line segments with an intersection. In order to make convenient contact with our above discussion for clusters without the vertex 20 (and its analogue on the odd sublattice), it now turns out that for eq. (66) the choice $\alpha = 1/2$ is to be made while for eq. (67) $\alpha = -1$ has to be selected[1]. If one does so the following simple rule for

---

[1]Clearly, the final result for the partition function does not depend on the choice of α; however

treating the vertex 20 (and its analogue on the odd sublattice) emerges. Replace in any vertex cluster under consideration each vertex 20 (and its analogue on the odd sublattice) by two line segments according to the graphical rule

$$\Huge + \qquad \longrightarrow \qquad \dashv\vdash \quad + \quad \daleth \quad + \quad \rceil_\lfloor \qquad . \tag{68}$$

Each of the line segments can be oriented, consequently each of the three terms on the r.h.s. of eq. (68) yields four different diagrams of two oriented line segments (twelve different terms in total). While clusters without the vertex 20 (and its analogue on the odd sublattice) contain self-avoiding ($k_l = 1$) thin line loops only, the last term on the r.h.s. of eq. (68) now allows ($k_l = 1$) thin line loops with intersections also. The weight of any of the twelve possible diagrams containing now instead of the vertex 20 two oriented ($k_l = 1$) thin line segments, passing each other without intersection or intersecting each other, can simply be calculated by taking separately the weights of each oriented line segment from eqs. (44)-(49) and multiplying them. This concludes the discussion of the vertex 20.

The rule for calculating the weight of a vertex cluster consequently is the following. Replace any vertex 20 (and its analogue on the odd sublattice) according to the rule (68) by two ($k_l = 1$) thin line segments (If P_{20} is the number of its occurrences in a given vertex cluster, this rule leads to $3^{P_{20}}$ different configurations. The latter term from now on always denotes the diagrams generated from a vertex cluster by application of the rule (68), or (72).). Provide any of the, say, m ($k_l = 1$) thin line loops (without reinterpreting thick lines as two parallel thin lines) with an orientation. This leads for a given configuration to 2^m different graphs (From now on the latter term denotes diagrams generated this way from configurations.). Represent the obtained graphs completely as a collection of, say, n oriented thin line loops (with thick lines interpreted as two oppositely oriented thin lines). In total, this leads for any original vertex cluster under consideration to different $3^{P_{20}} 2^m$ graphs with a certain number of oriented thin line loops each (this number may differ from graph to graph). Calculate the weight of each single oriented thin loop of length l by multiplying the weights of the l combinations of oriented line segments it is built of and attach the ordering factor -1. The weight of each graph is given by the product of the n oriented thin line loops it can be represented by. Any vertex cluster consequently has as weight the sum of the weights of the $3^{P_{20}} 2^m$ graphs generated from it.

---

the present choice admits a particularly simple way of describing contributions to the partition function.

In order to make further progress, first we have to study the weight of an arbitrary oriented thin line loop L. According to eqs. (44)-(49) the absolute value of the weight is given by the number of corners $C(L)$ of the loop as well as the number of occurrences of the vertices 21-26, denoted by P_M, and reads $2^{-C(L)/2} M^{P_M}$. According to the above considerations the sign of the loop weight is given by $(-1)^{(C_-(L)+1)}$, where $C_-(L)$ is the number of (oriented) right-up, up-right segments (cf. the second term on the r.h.s. of eqs. (46), (47)). Now, it is useful to take into account the equation

$$C_-(L) \equiv q(L) + 1 \ (\text{mod } 2) \ , \tag{69}$$

where $q(L)$ is the number of self-intersections of the loop L. A proof of eq. (69) can be found in Appendix A. From eq. (69) immediately follows that the weight of a thin line loop under consideration is given by[2]

$$(-1)^{q(L)} \, 2^{-C(L)/2} \, M^{P_M} \ . \tag{70}$$

This formula immediately also applies if L is understood to be a graph of, say, n thin line loops ($q(L)$ can still be understood as the number of intersections; however only self-intersections of loops are really important because the number of intersections of different loops is always even.). This graph of loops can exhibit 2^m different combinations of orientations if the configuration (obtained from a vertex cluster under consideration by application of the rule (68)) it is generated from contains m ($k_l = 1$) thin line loops. However, $q(L)$ may differ for these cases. Consequently, cancellations may and will occur among the $3^{P_{20}} \, 2^m$ graphs generated from a given vertex cluster. In the following subsection we continue with some observations in this respect.

2.3 From oriented to coloured loops

For the moment, in order to simplify the discussion let us only consider vertex clusters without any vertex 20. We show that any vertex cluster L under consideration containing a ($k_l = 1$) thin line loop with an odd number of the vertices 8-19 has vanishing weight. Let P_T be the number of the vertices 8-19 in a certain ($k_l = 1$) thin line loop A in L. Now, generate from any configuration with $P_T(A) \equiv 1 \ (\text{mod } 2)$ according to the procedure explained above 2^m graphs of oriented thin line loops (with thick lines interpreted as two oppositely oriented thin lines). There are, say, P_{T1} vertices 8-19 in the ($k_l = 1$) thin line loop A whose attached thick lines start

---

[2]Incidentally, P_M is always even. This can easily be seen for any given vertex cluster by simply dropping all thick lines from it, i.e. by replacing all vertices 8-19 by vertices 21-26.

and end at the loop A, consequently $P_{T1} \equiv 0 \pmod 2$. If these thick lines are interpreted as thin lines, the number of thin line intersections is zero (modulo 2). There are P_{T2} vertices 8-19 in the ($k_l = 1$) thin line loop A whose attached thick lines start at the loop A and end at some other ($k_l = 1$) thin line loop. If these thick lines are interpreted as thin lines, the number of thick lines starting from the loop A and containing one or zero (modulo 2) thin line intersections are P_{T2o} and P_{T2e} respectively. It holds

$$P_T(A) \;=\; P_{T1} \;+\; P_{T2o} \;+\; P_{T2e} \;\equiv\; 1 \;(\text{mod } 2) \quad . \tag{71}$$

Consequently, either P_{T2o} or P_{T2e} is odd (and the other is even, of course). If one now reverses the orientation of just the ($k_l = 1$) thin line loop A (with all other orientations fixed) the numbers P_{T2o} and P_{T2e} interchange (and $\Delta q = \Delta P_{T2o} \equiv 1 \pmod 2$ for the graphs with the opposite orientation of A). From eq. (70) one immediately recognizes that after summation over the two opposite orientations of the loop A the weight of any configuration containing A vanishes.

We now draw some first conclusions from the insight just obtained. We demonstrate that any vertex cluster L can be built by the overlap of two sets of self-avoiding loops (Self-avoidance here means that also intersections of different loops within a given set are not allowed.). We distinguish the loops out of the two different sets by attaching a colour, say red and blue, to each sort of loop. We proceed as follows. Divide any given ($k_l = 1$) thin line loop of a vertex cluster L into sections of alternating colour where the colour changes at any vertex 8-19 (This is possible, because any ($k_l = 1$) thin line loop contributing to the partition function contains an even number of vertices 8-19, as we have shown in the preceding paragraph.). This procedure yields two different colourings for each ($k_l = 1$) thin line loop in L (They just differ by an interchange between red and blue.). These two colourings stand in correspondence to the two different orientations of any ($k_l = 1$) thin line loop in L. We can then interpret any thick line in L as two parallel thin lines of different colour. It is clear that the described procedure yields a covering of the given vertex cluster L by two sets of self-avoiding, differently coloured loops (at each vertex meet, at most, two links of the same colour only). Consequently, in view of eq. (70), the weight of any vertex cluster (not containing any vertex 20) which is not zero must be positive. The graphs generated from vertex clusters with positive weight can be thought of as being constructed from the overlap of two differently coloured sets of self-avoiding loops (with monomer weight $z = M$ and bending rigidity $\eta = 1/\sqrt{2}$). Their weight is given by the product of the weights of the coloured loops they are built of. The number of different graphs corresponding to a vertex cluster is exactly given by the number of different coverings of it by means of two sets of differently coloured self-avoiding loops.

19

We would now like to extend the discussion to vertex clusters containing vertices of type no. 20. The best strategy to do so seems to be to transform any vertex cluster containing vertices of type no. 20 into "equivalent" vertex clusters without these (The problem we are interested in is primarily a topological one.). By "equivalent" we mean vertex clusters which have the same weight as the original one up to some positive constant which can easily be taken care of. The idea is to "stretch" any vertex 20 into two parts in such a way that in the "equivalent" cluster both parts are connected by a thick line. For any given column (row) of lattice points which contains a vertex 20 the "stretching" can be facilitated by inserting two additional lattice point columns (rows) to the left (top) and right (bottom) of the column (row) under consideration (The procedure is to be performed for each individual vertex 20 separately.). Pictorially, the procedure can be represented by the rule (for columns)

$$\tag{72}$$

Any other vertex 2-26 in the given column can also easily be "stretched" (shifted to the left or right) by appropriately inserting further horizontal thick or ($k_l = 1$) thin lines (and filling the remaining sites emerging in the "stretching" procedure by monomers). Although one might be tempted to do so, the rule (72) should not be confused with the rule (68) which has a different algebraic meaning in terms of combinations of Grassmann variables. It is however a way of dealing with the vertex 20 which is alternative to (68). Let us be more specific to illustrate (72). For example, for a vertex 20 on the even sublattice Λ_e one finds by means of the above procedure the expression (x denotes the coordinate of the vertex 20 on the "unstretched" lattice, which on the "stretched" lattice becomes the middle point of the introduced thick lines. On the "stretched" lattice the Grassmann integrations at the points $x - e_1$, x, $x + e_1$ have been carried out.)

$$- \chi_1(x + e_1 - e_2)\, \bar\psi_1(x + 2e_1)\, \chi_2(x - e_1 + e_2)\, \bar\psi_2(x - 2e_1)/2$$

$$- \psi_1(x - 2e_1)\, \bar\chi_1(x - e_1 + e_2)\, \chi_1(x + e_1 - e_2)\, \bar\psi_1(x + 2e_1)/2$$

$$- \psi_2(x + 2e_1)\, \bar\chi_2(x + e_1 - e_2)\, \chi_2(x - e_1 + e_2)\, \bar\psi_2(x - 2e_1)/2$$

$$- \psi_1(x - 2e_1)\, \bar\chi_1(x - e_1 + e_2)\, \psi_2(x + 2e_1)\, \bar\chi_2(x + e_1 - e_2)/2$$

$$- \chi_1(x - e_1 - e_2)\, \bar\psi_1(x + 2e_1)\, \chi_2(x + e_1 + e_2)\, \bar\psi_2(x - 2e_1)/2$$

$$- \psi_2(x + 2e_2)\, \bar\chi_1(x + e_1 + e_2)\, \chi_1(x - e_1 - e_2)\, \bar\psi_2(x - 2e_1)/2$$

$$- \psi_1(x - 2e_1) \, \bar{\chi}_2(x - e_1 - e_2) \, \chi_2(x + e_1 + e_2) \, \bar{\psi}_1(x + 2e_2)/2$$

$$- \psi_1(x - 2e_1) \, \bar{\chi}_1(x + e_1 + e_2) \, \psi_2(x + 2e_1) \, \bar{\chi}_2(x - e_1 - e_2)/2 \quad . \tag{73}$$

The first four terms correspond to the first term on the r.h.s. of (72) while the last four terms correspond to the second term on the r.h.s. of (72). If one shifts back each argument in (73) by either plus or minus e_1 one reobtains the expression on the r.h.s. of eq. (29). Let us also discuss the rule (72) from the point of view of a vertex 20 on the odd sublattice Λ_o. Some of the corresponding results read as follows (Again, the Grassmann integration has been performed at the points $x - e_1$, x, $x + e_1$, where x denotes the coordinates of the vertex 20 on the odd sublattice.).

$$\tag{74}$$

$$\tag{75}$$

In these equations we again apply the graphical conventions as explained previously (cf. eqs. (44)-(49), (55)). The equations (74), (75) relate to the first term on the r.h.s. of (72), analogous results can be given for the second term. Eq. (74) corresponds to eq. (66) (Remember that for the ordering choice selected in eq. (66) we have applied the weight $\alpha = 1/2$, consequently we find $-1/2$ on the r.h.s. of eq. (74).). Eq. (75) corresponds to the last two terms in eq. (67) (However, this time for the ordering choice selected in eq. (67) we have applied the weight $\alpha = 0$. Consequently, eq. (67) is exclusively interpreted as intersection of oriented straight line segments. The corresponding reordering of the Grassmann variables introduces a relative minus sign. Therefore, we find $1/2$ on the r.h.s. of eq. (75).).

The rule (72) now allows to efficiently handle the colouring problem for vertex clusters L containing vertex 20 and also to calculate their weights. For any given vertex cluster the rule (72) introduces $2^{P_{20}}$ different configurations free of any vertex 20. As discussed above the summation over orientations of $(k_l = 1)$ thin line loops for these configurations (i.e. the summation over graphs) lets only those survive which have an even number of vertices 8-19 in any $(k_l = 1)$ thin line loop. The sum of the weights of these configurations with non-vanishing (and consequently positive) weights yields the total weight of any vertex cluster containing vertices of type no. 20. For any graph generated from a configuration with nonvanishing weight the described colouring procedure can be carried out and then the rule (72)

can be reversed without any problem (It depends on the shape of the configuration whether both terms on the r.h.s. of (72) lead to diagrams with non-vanishing weight.). Consequently, the above insight for the calculation of the weight of vertex clusters without any vertex 20 immediately carries over to any configuration generated from an arbitrary vertex cluster. Finally, it is clear that any overlap of two sets of self-avoiding loops generates a vertex cluster constructed out of the vertices 2-26. The two possible orientations of ($k_l = 1$) thin line loops correspond to the colour exchange among the two sets (or, more precisely, to the exchange of the loop configurations among the two sets of different colour).

2.4   The two-colour loop model

We arrive at the following picture for the one-flavour Thirring model with Wilson fermions. Any diagram (and its weight) contributing to the partition function Z_Λ can be regarded as being generated by the overlap of two differently coloured sets of self-avoiding loops with monomer weight $z = M$ and bending rigidity $\eta = 1/\sqrt{2}$. Only the monomer weight $M^2 - 2G$ (eq. (10)) of the Thirring model differs from the product of the monomer weights of the two differently coloured self-avoiding loop models M^2. However, for free fermions ($G = 0$) there is complete agreement. Consequently, the structure of the statistical model equivalent to the Thirring model with Wilson fermions is very close to that for a free Dirac fermion. Therefore, for $G = 0$ we find

$$Z_\Lambda \;=\; \left(Z_\Lambda \left[M, \frac{1}{\sqrt{2}} \right] \right)^2 \; , \tag{76}$$

where $Z_\Lambda[z, \eta]$ is the partition function for the self-avoiding loop model with monomer weight z and bending rigidity η as defined in [15] (see also further below). This result is not astonishing because the self-avoiding loop model with bending rigidity $\eta = 1/\sqrt{2}$ is known [16] (see also [17]), [18] to be a free fermion model [19], [20] (cf. also sect. 4 of [15]). The model has second order phase transitions (within the Ising model universality class) at $z = M = 2$ (this corresponds to $\kappa = 1/4$) and $z = M = 0$ (where it is equivalent to a 6-vertex model). At $z = M = 0$ the central charge c of the self-avoiding loop model with bending rigidity $\eta = 1/\sqrt{2}$ is $c = 1$ [21], [22] while, as has been argued in [15], at $z = M = 2$ it should have $c = 1/2$ which is rather obvious from eq. (76) because any free Dirac fermion has $c = 1$.

Let us now specify in detail the statistical model equivalent to the one-flavour lattice Thirring model with Wilson fermions (and Wilson parameter $r = 1$). This statistical model is a two-color loop model with bending rigidity $\eta = 1/\sqrt{2}$ and
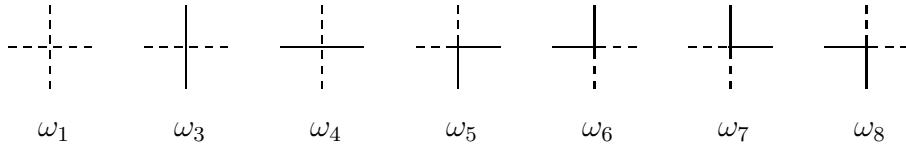
Figure 1: Vertices of the (one-colour) self-avoiding loop model (The intersection vertex is omitted because its weight ω_2 is zero.). Loop segments are denoted by continuous lines.

monomer weight $M^2 - 2G$. The vertices and weights of this model can best be described as follows. Consider the (one-colour) self-avoiding loop model with monomer weight $z = M$ and bending rigidity $\eta = 1/\sqrt{2}$ (For the vertices see Fig. 1.). The weights are

$$\omega_1 \;=\; z \;=\; M \quad , \tag{77}$$

$$\omega_3 \;=\; \omega_4 \;=\; 1 \quad , \tag{78}$$

$$\omega_5 \;=\; \omega_6 \;=\; \omega_7 \;=\; \omega_8 \;=\; \eta \;=\; \frac{1}{\sqrt{2}} \quad . \tag{79}$$

This model is a special 8-vertex model (with $\omega_2 = 0$, i.e. a 7-vertex model) and, therefore, we have applied here the standard 8-vertex model notation (for a discussion of the model also see [15]). The vertices of the two-colour loop model equivalent to the Thirring model can now be found by taking two differently coloured sets of the vertices shown in Fig. 1 and overlapping them in any possible way. This leads to 49 two-colour loop model vertices (because each one-colour loop model has seven vertices with non-vanishing weight). The weights of 48 out of the total 49 of these two-colour vertices are simply given by the product of the weights of the one-colour vertices they are built of. The only exception is the overlap of the two one-colour monomer vertices (which is the two-colour monomer vertex) which has the weight $M^2 - 2G$ instead of M^2 (cf. eq. (10)).

3   Discussion and conclusions

The value $c = 1$ of the central charge c of the one-flavour Thirring model, which is independent of the coupling G, has been discussed by various methods in [23], [24], [25]. With the concept of universality in mind, this result is not surprising since a

variation of G only affects the monomer weight of the two-colour loop model equivalent to the Thirring model, consequently at least in a certain vicinity of $G = 0$ the Thirring model should be expected to exhibit the same value of the central charge as free Dirac fermions.

Let us also comment on the relation of the above two-colour loop model to other statistical systems. Somewhat similar two-colour loop models have recently been discussed in [26]. Furthermore, the two-colour loop model equivalent to the Thirring model can also be viewed as a 4-state vertex model. To see this note that the one-colour self-avoiding loop model, whose vertices are shown in Fig. 1, is a 2-state model. This leads, by construction, to the understanding of the Thirring model as a 4-state 49-vertex model. Q-state vertex models have been studied, e.g. in [27]-[36]. However, the particular 4-state models discussed in [28], [35], [36] do not contain the case of the 4-state vertex model equivalent to the Thirring model which seems to not have been investigated in the published literature on the subject (except, in view of eq. (76), the free fermion case, where one may use the results obtained in [37]). Finally, it is interesting to note, just as an aside, that also certain other models with four states have recently been discussed within the context of fermionic systems in [38], [39].

The present investigation also immediately allows to draw conclusions about another lattice model, namely the one-flavour strong (infinite) coupling Schwinger model with an additional four-fermion interaction term (i.e. the Thirring-Schwinger model with some finite four-fermion coupling constant G as in the Thirring model itself). For $G = 0$ Salmhofer has found the exact equivalence of this model to a (one-colour) self-avoiding loop model with monomer weight $z = M^2$ and bending rigidity $\eta = 1/2$ [5]. From our consideration of the Thirring model immediately follows, that for $G \neq 0$ one only has to replace the monomer weight $z = M^2$ by $z = M^2 - 2G$ in order to obtain the corresponding equivalence. Consequently, the model can be discussed along exactly the same lines as done for $G = 0$ in [15].

To conclude, in the present article we have found the exact equivalence of the one-flavour lattice Thirring model with Wilson fermions and Wilson parameter $r = 1$ to a two-colour loop model which can also be viewed as a 4-state 49-vertex model on the square lattice. The choice $r = 1$ has proved crucial in simplifying the analysis. It should be emphasized that the two-colour loop model is a statistical model with positive weights which allows its numerical simulation by standard methods. The loop model picture even might prove advantageous because it allows the application of efficient cluster algorithms (e.g. see [40], [41]). The particular loop model equivalence found for free fermions (cf. eq. (76)) might be helpful in the future analysis of multi-flavour four-fermion models in 2D. Also, it might serve as a suggestive starting

point for the further analysis of Wilson fermions in higher dimensions.

Acknowledgements

Appendix A

In this Appendix we demonstrate that the relation

$$C_-(L) \quad \equiv \quad q(L) + 1 \ (\text{mod } 2) \tag{A.1}$$

holds, where $q(L)$ is the number of self-intersections of a given thin line loop L and $C_-(L)$ is the number of (oriented) right-up, up-right segments (cf. the second term on the r.h.s. of eqs. (46), (47)). We only consider loops which do not occupy a link twice which, in principle, is possible due to links with $k_l = 2$ (thick lines). One may always put such loops which visit at least one link twice on a finer lattice where each link can be occupied only once. The analysis demonstrating the validity of eq. (A.1) consequently can also be extended to such cases.

We start with $q = 0$. The proof will be based on an induction with respect to the area $\Omega(L)$ enclosed by the loop L. If the area $\Omega(L)$ of L is one (in lattice units), i.e. $|L| = 4$ ($|L|$ is the length of the loop), one may convince oneself that eq. (A.1) holds ($C_- = 1$ in this case). Consider now a loop L with $\Omega(L) > 1$. There exists at least one loop L' with $\Omega(L') = \Omega(L) - 1$ whose interior differs from L by just one lattice square (This selection of L' is important because otherwise certain transformations to be discussed below would possibly not apply.). Consequently, we may perform a deformation of the loop L' into the loop L. We will demonstrate that in such a transformation $\Delta C_- = C_-(L') - C_-(L) \equiv 0 \ (\text{mod } 2)$ holds. In the transformation a lattice square is added to the interior of the loop L' which has at least one boundary link belonging to the loop L'. There are three different cases to be considered: the lattice square under consideration either has one ((A.2)), two ((A.3)) or three ((A.4)) boundary links belonging to the loop L' (In the case of two links we do not need to consider the case where two opposite sites of the lattice square belong to the loop L' because this would be in contradiction with our choice for L'.). Below we depict some of the situations that may occur. The complete set is obtained by rotating the pictures in (A.2)-(A.4) in all possible ways.

$$\tag{A.2}$$

$$\tag{A.3}$$

$$\text{(A.4)}$$
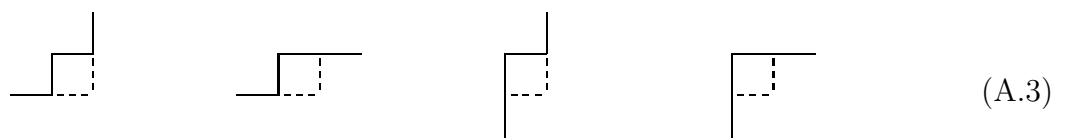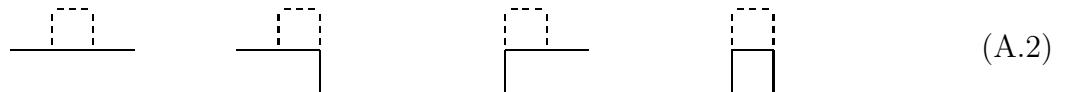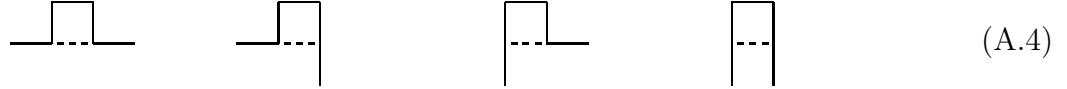
One may now provide the loop segments in (A.2)-(A.4) with an orientation (L' is denoted by a continuous line.). Then, for each possible case one may explicitly convince oneself that in the transition from the loop L' to the loop L $\Delta C_- \in \{-2, 0, 2\}$. According to our induction assumption eq. (A.1) holds for the loop L' ($\Omega(L') = \Omega(L) - 1$), consequently it also holds for L. Therefore, eq. (A.1) is valid for any loop with $q = 0$. Now we are prepared to discuss the case $q > 0$ (I am indebted to C. Krattenthaler for the argument [42].). We perform an induction with respect to q. The case $q = 0$ has just been considered. Next, assume a given oriented loop L has $q(L) > 0$ self-intersections. Select a certain intersection and apply to it a reinterpretation in terms of two oriented line segments passing each other without intersection. This leads to two different loops A and B with $q(A) < q(L)$ and $q(B) < q(L)$ intersections each ($q(A) + q(B) = q(L) - 1$). As one may convince oneself easily, in this operation in three of the four different cases the total number of (oriented) right-up, up-right segments does not change. C_- only goes up by 2 in the case of the following intersection diagram.

$$\text{(A.5)}$$

Consequently, within the considered operation C_- remains constant modulo 2. Now, according to our induction assumption eq. (A.1) is valid for the loops A and B, therefore

$$C_- \equiv [q(A) + 1] + [q(B) + 1] \equiv q(L) + 1 \ (\text{mod } 2) \, . \tag{A.6}$$

This proves eq. (A.1).

27

References

[1] B. Rosenstein, B.J. Warr, S.H. Park; Phys. Rep. **205**(1991)60.

[2] S. Hands, A. Kocić, J.B. Kogut; Ann. Phys. (N.Y.) **224**(1993)29.

[3] C.N. Leung, S.T. Love, W.A. Bardeen; Nucl. Phys. **B 273**(1986)649.

[4] C.N. Leung, S.T. Love, W.A. Bardeen; Nucl. Phys. **B 323**(1989)493.

[5] M. Salmhofer; Nucl. Phys. **B 362**(1991)641.

[6] K. Scharnhorst; University of Wales Swansea, Preprint SWAT/96/105, hep-lat/9604024, Nucl. Phys. **B 479**[FS](1996)727, to appear.

[7] P. Rossi, U. Wolff; Nucl. Phys. **B 248**(1984)105.

[8] V.E. Korepin, N.M. Bogoliubov, A.G. Izergin; Quantum Inverse Scattering Method and Correlation Functions. Cambridge University Press, Cambridge, 1993, sect. III, p. 80.

[9] Y.K. Zhou, K.D. Schotte; Phys. Rev. **D 47**(1993)R1281.

[10] S. Coleman; Phys. Rev. **D 11**(1975)2088.

[11] A. Luther; Phys. Rev. **B 14**(1976)2153.

[12] M. Lüscher; Nucl. Phys. **B 117**(1976)475.

[13] K. Ishida, S. Saito; Prog. Theor. Phys. **74**(1985)113.

[14] Wolfram Research; Mathematica, version 2.2. Wolfram Research, Champaign, 1994.

[15] K. Scharnhorst; University of Wales Swansea, Preprint SWAT/95/72, hep-lat/9505001.

[16] V.B. Priezzhev; Zh. Eksp. Teor. Fiz. **74**(1978)1177. English translation: Sov. Phys. JETP **47**(1978)619.

[17] E.I. Kornilov, V.B. Priezzhev; J. Phys. **A 18**(1985)L251.

[18] T. Blum, Y. Shapir; J. Phys. **A 23**(1990)L511.

[19] C. Fan, F.Y. Wu; Phys. Rev. **179**(1969)560.

[20] C. Fan, F.Y. Wu; Phys. Rev. **B 2**(1970)723.

[21] H.J. de Vega, M. Karowski; Nucl. Phys. **B 285**[FS19](1987)619.

[22] M. Karowski; Nucl. Phys. **B 300**[FS22](1988)473.

[23] C. Destri, H.J. de Vega; Phys. Lett. **B 223**(1989)365.

[24] S.S. Xue; Nuov. Cim. **A 103**(1990)1535.

[25] B.W. Xu; Comm. Theor. Phys. **15**(1991)383.

[26] S.O. Warnaar, B. Nienhuis; J. Phys. **A 26**(1993)2301.

[27] Yu.G. Stroganov; Phys. Lett. **A 74**(1979)116.

[28] V.A. Fateev; Yad. Fiz. **33**(1981)1419. English translation: Sov. J. Nucl. Phys. **33**(1981)761.

[29] J.H.H. Perk, C.L. Schultz; Phys. Lett. **A 84**(1981)407.

[30] J.H.H. Perk, C.L. Schultz, in: M. Jimbo, T. Miwa (Eds.): Non-linear Integrable Systems — Classical Theory and Quantum Theory, Proc. of RIMS Symposium organised by M. Sato, Kyoto, Japan, 13-16 May 1981. World Scientific, Singapore, 1983, p. 135.

[31] K. Sogo, Y. Akutsu, T. Abe; Prog. Theor. Phys. **70**(1983)730, *ibid.* 739.

[32] J.H.H. Perk, C.L. Schultz; Physica **A 122**(1983)50.

[33] J.H.H. Perk, F.Y. Wu; Physica **A 138**(1986)100.

[34] H.J. Giacomini; Phys. Lett. **A 117**(1986)381.

[35] Y. Akutsu, M. Wadati; J. Phys. Soc. Jpn. **56**(1987)3039.

[36] R.M. Kashaev, V.V. Mangazeev; Phys. Lett. **A 150**(1990)375.

[37] V.V. Bazhanov, Yu.G. Stroganov; Teor. Mat. Fiz. **62**(1985)377, *ibid.* **63**(1985)291, *ibid.* **63**(1985)417. English translation: Theor. Math. Phys. **62**(1985)253, *ibid.* **63**(1985)519, *ibid.* **63**(1985)604.

[38] G.N. Ord; J. Stat. Phys. **66**(1992)647.

[39] H. Hinrichsen; J. Phys. **A 27**(1994)5393.

[40] I. Montvay, G. Münster; Quantum Fields on a Lattice. Cambridge University Press, Cambridge, 1994, sect. 7.7, p. 427.

[41] H.G. Evertz, G. Lana, M. Marcu; Phys. Rev. Lett. **70**(1993)875.

[42] C. Krattenthaler, private communication.